NAVAL POSTGRADUATE SCHOOL
Monterey, California

THESIS

AN APPROACH FOR STUDYING THE CREEP/ SLIDING BEHAVIOR OF PLANAR METAL-SILICON INTERFACE

by

Ioannis Farsaris

December 1999

Thesis Advisor: Indranath Dutta

Approved for public release; distribution is unlimited.

REPORT DOCUMENTATION PAGE

Form Approved OMB No. 0704-0188

1. AGENCY USE ONLY *(Leave blank)*	2. REPORT DATE	3. REPORT TYPE AND DATES COVERED
	December 1999	Engineer's Thesis

4. TITLE AND SUBTITLE
AN APPROACH FOR STUDYING THE CREEP/SLIDING BEHAVIOR OF PLANAR METAL-SILICON INTERFACES

5. FUNDING NUMBERS

6. AUTHOR(S)
Lieutenant J.G Ioannis Farsaris

7. PERFORMING ORGANIZATION NAME(S) AND ADDRESS(ES)
Naval Postgraduate School
Monterey, CA 93943-5000

8. PERFORMING ORGANIZATION REPORT NUMBER

9. SPONSORING / MONITORING AGENCY NAME(S) AND ADDRESS(ES)

10. SPONSORING / MONITORING AGENCY REPORT NUMBER

11. SUPPLEMENTARY NOTES
The views expressed in this thesis are those of the author and do not reflect the official policy or position of the Department of Defense or the U.S. Government.

12a. DISTRIBUTION / AVAILABILITY STATEMENT
Approved for public release; distribution is unlimited.

12b. DISTRIBUTION CODE

13. ABSTRACT *(maximum 200 words)*

There has been considerable recent interest in interfacial sliding during creep of multi-phase materials. The effect of interfacial creep is crucial for the deformation of metal-matrix composites and thin film systems, where the isostrain condition between the constituent components is often violated. An experimental approach has been developed to investigate the deformation kinetics of planar interfaces, using a double-shear specimen geometry where the interfaces are loaded in shear. In addition to shear stresses, the apparatus is capable of applying normal stresses (tension or compression) on the interface. In the experimental arrangement, the relative displacements of the constituents at the top and bottom of the specimen are measured independently with high precision using a resistance gauge and a capacitance sensor, respectively. The experimental set-up is suitable for both constant displacement-rate and constant-load creep tests, and can be operated up to a temperature of 500°C. In the current study, preliminary creep tests were conducted on planar aluminum-silicon interfaces prepared by diffusion bonding in argon atmosphere at 565°C. During the tests, the interfaces were subjected to nominally constant shear stresses ranging from 0.8-2 MPa, with the test temperatures ranging from 100-200°C. In all cases, the interface was found to slide via a time-dependent relaxation mechanism, indicating the suitability of the proposed test for studying interfacial sliding. Further studies are needed to determine the mechanistic details of interfacial sliding.

14. SUBJECT TERMS
Composite, Planar Interface, Interfacial Sliding, Creep.

15. NUMBER OF PAGES
65

16. PRICE CODE

17. SECURITY CLASSIFICATION OF REPORT	18. SECURITY CLASSIFICATION OF THIS PAGE	19. SECURITY CLASSIFICATION OF ABSTRACT	20. LIMITATION OF ABSTRACT
Unclassified	Unclassified	Unclassified	UL

NSN 7540-01-280-5500

Standard Form 298 (Rev. 2-89)
Prescribed by ANSI Std. 239-18

Approved for public release; distribution is unlimited

AN APPROACH FOR STUDYING THE CREEP/SLIDING BEHAVIOR OF PLANAR METAL-SILICON INTERFACES

Ioannis Farsaris
Lieutenant J.G., Hellenic Navy
B.S., Hellenic Naval Academy, 1992

Submitted in partial fulfillment
of the requirements for the degree of

MASTER OF SCIENCE IN MECHANICAL ENGINEERING
and
MECHANICAL ENGINEER

from the

NAVAL POSTGRADUATE SCHOOL
December 1999

Author: _____
Ioannis Farsaris

Approved by: _____
Indranath Dutta., Thesis Advisor

_____
Terry R. McNelley, Chairman
Department of Mechanical Engineering

ABSTRACT

There has been considerable recent interest in interfacial sliding during creep of multi-phase materials. The effect of interfacial creep is crucial for the deformation of metal-matrix composites and thin film systems, where the isostrain condition between the constituent components is often violated. An experimental approach has been developed to investigate the deformation kinetics of planar interfaces, using a double-shear specimen geometry where the interfaces are loaded in shear. In addition to shear stresses, the apparatus is capable of applying normal stresses (tension or compression) on the interface. In the experimental arrangement, the relative displacements of the constituents at the top and bottom of the specimen are measured independently with high precision using a resistance gauge and a capacitance sensor, respectively. The experimental set-up is suitable for both constant displacement-rate and constant-load creep tests, and can be operated up to a temperature of 500°C. In the current study, preliminary creep tests were conducted on planar aluminum-silicon interfaces prepared by diffusion bonding in argon atmosphere at 565°C. During the tests, the interfaces were subjected to nominally constant shear stresses ranging from 0.8-2 MPa, with the test temperatures ranging from 100-200°C. In all cases, the interface was found to slide via a time-dependent relaxation mechanism, indicating the suitability of the proposed test for studying interfacial sliding. Further studies are needed to determine the mechanistic details of interfacial sliding.

TABLE OF CONTENTS

ACKNOWLEDGMENTS

I would like to express my sincere gratitude and appreciation to Dr. Indranath Dutta for his persistence and guidance during the course of this thesis.

Special acknowledgment is due to Dr MingWei, for his contribution of time in laboratory assistance. I also acknowledge the partial financial support that was provided by the National Science Foundation under Contract # DMR 9423668.

Finally, I would like to thank my parents, Emmanouil and Eleftheria, who provided the most important things in life, love and support.

I. INTRODUCTION

In industrial fabrications, selection of materials plays an essential role in the performance of the final product. Whatever the field of design engineering, the final limitation on advancement depends on the material properties. The combination and engineering of the constituent materials, introduces new factors in the total design, that have to be taken into consideration in order to achieve the required level. Material interfaces are almost everywhere, produced by this combination. Material interfaces can be found in metal-matrix composites, ceramic-matrix composites, polymer-matrix composites, thick and thin film coatings, multi-phase alloys, and in electronic devices. From the above is clear that interfaces can be between different materials, same materials or just between phases of the same material.

Structural components of metal-ceramic composites are widely used in many engineering applications, such as high-temperature propulsion systems, aerospace structure parts, automotive engine parts and wear resistant coatings. Metal-matrix and ceramic-matrix composites have enhanced performance characteristics at elevated temperatures when compared with similar low density, high strength alloys.

Multilayers of metals and ceramics are also used in the microelectronics industry were the trend is leading to more compact and complex components that can withstand higher temperatures. The fabrication of composite components and semiconductor device structures depends strongly on the performance of the interfaces. The performance reliability and yield increases proportionately with the complexity of the structure or the component and with the environmental conditions that are used. In electronic packaging,

design engineers are tailoring the thermal expansion coefficient and thermal conductivity of the materials used, so as to achieve electronic devices that have almost exotic properties.

The performance of the interface has different characteristics when the temperature is changing and thermal stresses are introduced. The creep behavior becomes important and the need to categorize the mechanisms that influence this behavior is vital for the prediction of the overall performance. In studying the creep behavior of composites and other multi-phase systems, various models have been introduced, that treat the interfaces as being perfectly bonded and non-sliding, leading to an isostrain condition between the constituent phases [Ref. 3, 5]. Under these conditions the models predict extensive plastic flow during thermal cycling and strong dependence on the rates of heating and cooling. However, isostrain condition at the interface have been shown to be violated frequently. For instance, it has been shown [Ref. 3, 6] that following thermal cycling experiments the fibers in a metal-matrix composite may either protrude or intrude with respect to the matrix, depending on the rate of cycling, even though there was no fracture of the interface. Clearly, in this case, the matrix and fiber have slid relative to each other by interface creep.

Many experimental works have been done to study the behavior of interfaces in composites when there is a breakdown of the isostrain conditions. Most of them have assumed partial or total debonding of the interface and have considered interfacial sliding to be controlled by frictional resistance to the relative displacement of the two materials involved [Ref. 7, 8, 9]. Recently it has been shown [Ref. 7, 13, 15] that for well bonded

interfaces, frictional sliding is not the primary mechanism of interfacial sliding, especially at higher temperatures. Diffusional accommodation at the interface was introduced [Ref. 7, 13, 15] to explain the sliding of interfaces without debonding. Tests under various combinations of load and temperature have been conducted in order to explain the behavior of the interface [Ref 7].

Since the behavior of the interface is critical to the behavior of the whole composite, it is important to isolate and measure the deformation characteristics. So far, studies of the kinetics of interfacial sliding have been conducted on fiber composites [Ref. 7]. These experiments are constrained by the fact that there are strong thermal residual stresses present in a composite matrix which produce both interfacial shear and normal stresses. While the effect of the residual shear stresses may be minimized by proper design of the test samples, the normal stresses are always present and influence the interfacial strain response considerably [Ref. 7]. This limitation may be overcome by conducting experiments on model planar interfaces, where the normal stresses can be controlled independently.

Therefore, the purpose of this study is to formalize an approach for studying interfacial creep kinetics using model planar interfaces, wherein the interfacial shear and normal stresses may be controlled independently, and the resulting interfacial displacement may be accurately measured.

THIS PAGE INTENTIONALLY LEFT BLANK

II. BACKGROUND

A. INTERFACIAL SLIDING OBSERVATION IN ENGINEERING SYSTEMS

The importance of the interfaces to the overall performance of engineering systems was introduced in the previous chapter. Here some examples of these systems will be discussed to obtain a better understanding of the nature of interfacial creep.

An early work in slow thermal cycling of a composite is shown in Figure **1**, where the Cu matrix expanded and the fibers were intruding into the matrix with the extend of intrusion increasing with increasing the number of cycles. This work was the first to show, that isostrain conditions in composites are not necessarily valid, and interfacial sliding can occur even in the absence of interfacial fracture.

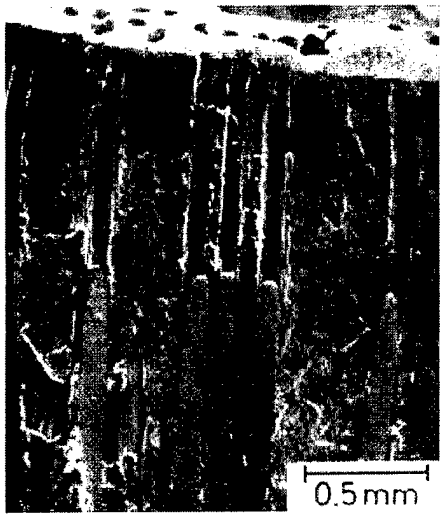

Figure 1. Cu matrix protruding beyond the ends of W-fibers after thermal cycling [Ref.5]

Later experiments on thermal cycling by Dutta *et al* [Ref. 4] showed similar effects where graphite fibers in aluminum matrix, Figure **2**, were intruding following

slow thermal cycling. The rate of heating/cooling during cycling, in conjunction with the tensile matrix residual stress along the fiber-axes, allowed the matrix to elongate relative to the fibers without any evidence of fracture.

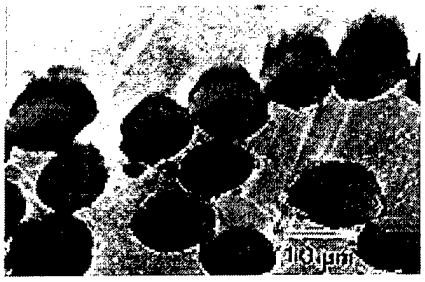

Figure 2. Intrusion of Graphite fibers in Al matrix [Ref. 4]

Time-dependent diffusional sliding at the interface close to fiber ends accommodates the differential strain between the fibers and the matrix. This diffusional flow is possible due to large interfacial shear stresses that exist, because of the difference of the thermal expansion coefficients between the fiber and the matrix. This is in agreement with the shear-lag model where load is transferred from the matrix to the fiber via the interfacial shear stress present only at the ends of the fibers.

On the other hand, the effects during relatively rapid thermal cycling are very different. Interfacial fracture was observed in experiments of rapid cycling by Mitra *et al* [Ref. 6] where fibers were protruding relative to the matrix as a result of the relief of axial compressive residual stresses in the fiber following interface fracture. The rapid thermal cycling was too fast for diffusional flow to occur and fracture of the interface was followed by frictional sliding as seen in Figure **3**. Frictional sliding is commonly observed in composites with weak interfaces, which undergo debonding during cycling.

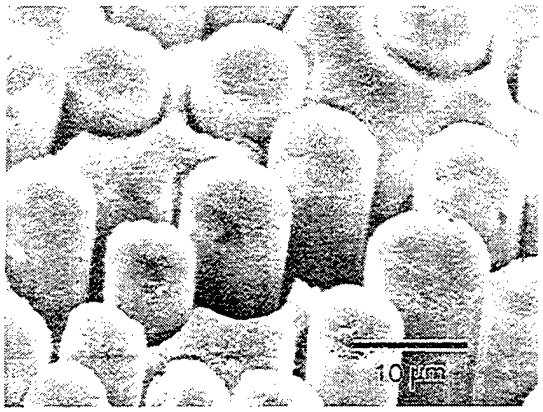

Figure 3. Interfacial debonding after rapid cycling [Ref. 6]

It is well known that mechanical properties of thin films differ greatly from those of bulk materials. Although creep behavior is similar, and experiments of creep on multilayers show the same mechanisms of interfacial sliding. Recently, during thermal cycling of high density interconnects (HDIC) showed diffusional accommodation of interfacial sliding [Ref. 10]. On this structure parallel Cu interconnect lines separated by polyimide (PI) dielectrics are deposited on a Si device, with tantalum (Ta) as a diffusion barrier at the Si-PI, Si-Cu and Cu-PI interfaces. A single layer structure based on Cu/PI HDIC is schematically shown in Figure 4.

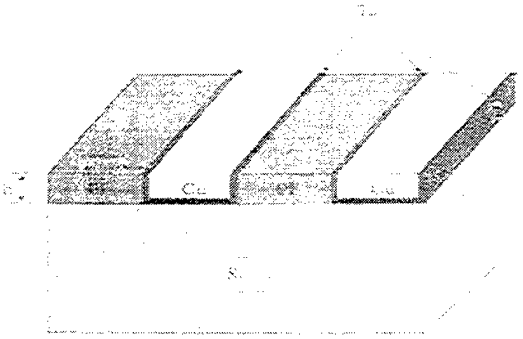

Figure 4. Schematic of Cu/PI HDIC on Si with Ta interlayers [Ref. 10]

Multi-level structures with Cu/PI HDICs have also been developed, where successive metal-dielectric layers are deposited on top of each other. During the processing steps involved in forming each layer (imidization and Cu deposition), the structure is heated to 350^0C (corresponding to ~$0.45T_m$ for Cu), thereby subjecting the entire package to thermal cycling conditions.

The study of the surface of a single HDIC layer by an atomic force microscopy (AFM) revealed significant height changes of the adjacent Cu and polyimide lines. These relative height differences are a result of in-plane deformation due to the large CTE mismatch between the PI, Ta and Cu. The deformation mechanisms is attributed to diffusionally accommodated sliding driven by shear stresses generated by the CTE mismatch, followed by relaxation by out-of plane stresses. Here, again, the amount of sliding strongly depends on the width of the Cu lines, similar to the shear stress transfer (shear-lag model) of the matrix to the fiber in the composites.

A similar work on multilayered materials by Shen *et al* [Ref. 11] was presented for analyzing the creep response and its underlying mechanisms under monotonic or cyclic variations in temperature. They produced two model systems, one of Al-Al_2O_3 bilayer and one trilayer of Al_2O_3-Al-Al_2O_3 with 1mm and 1μm thickness of the Al layer. The range of temperatures was from 20^0-450^0C so appreciable creep occurs in the Al layer while the Al_2O_3 layer remains primarily elastic with a negligible total strain rate at all times.

The thermally induced deformation of the multilayers was accurately predicted for the thick Al layer (resulting in curvature of the layer), while for the 1μm thickness the

stresses were fully relaxed. Interfacial sliding of the thin Al layer was proposed in order to achieve the stress relaxation during heating and cooling, when the rate was slow. The observed stress relaxation was explained by either Nabarro-Herring creep or Coble creep, depending the range of temperature of the sample. Especially at high temperatures they found, that steady state conditions were questionable since they were lacking one constitutive equation to describe the transient conditions.

From the above cited experimental works, it is evident that the effect of interfacial creep has often been difficult to recognize because of other concurrent and superimposed phenomena. In addition to that, high strain rate superplasticity in ceramics has been suggested to be controlled by interfacial sliding [Ref. 12]. The proposed mechanism suggested that sliding between matrix grains is accommodated by diffusionally accommodated sliding at the interface. In their results, the high activation energy for superplasticity was attributed to diffusion along particle-matrix interface.

B. MECHANISMS OF INTERFACIAL SLIDING

In the systems described above, creep relaxation of interfaces at high temperatures has often been difficult to define because of other concurrent and superimposed phenomena. Indirect evidence of diffusionally accommodated interfacial sliding due to the presence of interfacial stresses has been observed in many systems and explanations for the kinetics are varying considerably. In addition to the examples cited above, interfacial sliding has been also observed in dispersion strengthened metals [Ref. 13], intermetallics [Ref. 31], eutectic alloys [Ref. 32], film-sudstrate interfaces [Ref. 17], and

in various metals and ceramic-matrix composites [Ref. 33, 34]. In most systems, interface sliding controlled creep results in a stress exponent n ranging from 1 to 2 [Ref. 7, 13, 17, 31, 32]. It has also been observed a temperature dependent threshold stress, below which creep does not occur [Ref. 7, 35], and values for the activation energy varies from well over that for matrix volume diffusion Q_{vol} [Ref. 13] to below Q_{vol} [Ref. 7, 17, 31]. These discrepancies are somehow expected, since in the above mentioned works, the kinetics of interface sliding were inferred from the overall strain response of the entire materials system. In none of them, the interfacial sliding response was explicitly studied by isolating it from concurrent and superimposed effects.

The various mechanisms that have been proposed to explain interfacial creep can be categorized in five different formulas. First, grain boundary sliding is possible by diffusional creep. This to happen, the interface has to act as a perfect source and sink of vacancies due to a high number of mobile boundary dislocations. The rate of sliding then is determined by the rate these dislocations move across the interface [Ref 13]. In the strain rate equation then, the exponent becomes approximately 1, and the activation energy, depending the temperature, equals that for lattice diffusion (Nabarro-Herring creep), or boundary diffusion (Coble creep). In the case the density or mobility of dislocations in the boundary is limited, the kinetics describing the creep regime are believed to become "interface reaction controlled" [Ref. 13] where a threshold stress corresponds to the minimum stress required to move the boundary dislocations. The exponent of the strain rate equation becomes two and the activation energy is found to

take values much higher than that corresponding to the energy required to rearrange atoms on the stiffer side of the interface.

The second mechanistic formula refers in fibrous metal-matrix composites. The approach to describe the mobility of dislocations (or transfer of mass) follows a different way. The interface is thought of as a highly dislocation region of the matrix (a work hardened zone), formed due to the difference in stiffness between the fibers and the matrix. Dislocation reaction products and dislocation loops surround the fibers and stand off at some equilibrium distance, increasing so the work hardened zone. A recovery process follows driven by the movement of dislocations along the fiber towards the ends or by a dislocation annihilation processes [Ref. 14, 15]. This recovery process along with the formation of dislocations contributes to a flow of matter around the ends resulting in differential strain rates between the fiber and the matrix. The creep regime is described by power-law creeping where the exponent of the strain rate is approximately 4.5 [Ref. 14, 15].

The third formula follows a different way of approach. Interfacial sliding is made possible by two independent but related mechanisms [Ref. 16, 18]. First, the interface is thought to slide in shear with a linear rheology, due to the creeping of the interface layer by diffusion flow [Ref. 7]. Secondly, short-range interfacial diffusion contributes to a mass transfer, driven by gradients normal to the interface or by hydrostatic stress state due to the presence of interfacial asperities [Ref. 3]. Studies made by Kim *et al* [Ref. 16] on short fiber metal-matrix composites show that both mechanisms (viscous drag and diffusional flow) have the same linear stress dependence and the same direction of net

mass flow, suggest that it may be possible to combine the effects of both shear and normal stresses into one constitutive law.

The fourth formula has observed in lamellar TiAl alloys with a refined microstructure [Ref. 31]. Experiments involving creep deformation at low applied stresses and intermediate temperatures showed a nearly linear creep behavior. At these conditions, lattice dislocation movement and multiplication is very limited. Preexisting interfacial dislocations on the other hand, on both γ/α_2 and γ/γ interfaces, glide on a cooperative way predominating in the interfacial sliding. The glide rate was postulated to be limited by climb of sessile jogs and/or solute drag from interstitial impurities on the interface plane. The measured activation energy was found low, close to the activation enthalpies for diffusion of oxygen in TiAl and Ti. This, along with the linear relationship of dislocation velocity to the applied stress, supports the drag effect of interfacial dislocations (the viscous glide of interfacial dislocations is dragged by solute atoms controlling the whole creep deformation) [Ref 31].

The fifth formula/mechanism introduced by Jobin *et al* [Ref. 17], considers interfacial sliding to occur due to interaction between interfacial dislocations and lattice dislocations in one of the phases, resulting in a dislocation slip controlled sliding process with n approaching infinity. This mechanism is similar to the one discussed above in the fiber composites, except that, the rate controlling mechanism between the two phases is dislocation slip, rather than climb-glide motion. The experiments were contacted on a ductile substrate (copper) and a brittle film (silica) deformed under various strain-rate conditions. The ductile substrate was under tension and interfacial shear is transferring

the load to the silica film. As the strain was increased, cracks were developed on the brittle film with their spacing depended on the extent of interfacial sliding. It was suggested that at high strain rates / low temperatures, sliding is accommodated by dislocation slip, either by lattice dislocations and /or by dislocations in the plane if the interface itself. At low strain rates / high temperatures sliding occurs by diffusional flow with interface diffusion to be the dominant one [Ref. 17]. Further, it was suggested that interfacial sliding is unlikely to display power-law kinetics (climb-glide), since this is usually associated with sub-grain formation, and interfacial sliding is generally confined to a region much narrower than typical sub-grain sizes. However, some of the previous discussed mechanisms of interfacial sliding are based on a power-law formulation. This discrepancy reflects a fundamental confusion that exists on the mechanism of interfacial sliding.

In all the above studies, two distinguishable methodologies were used to infer interfacial creep kinetics. First, the overall strain response of the material was measured, the appropriate kinetics data were plotted, and from that the interfacial sliding kinetics were deducted, assuming it to be the rate controlling mechanism [e.g. Ref. 12,17]. Second, assuming an interfacial flow law, followed by modeling of the deformation behavior of the entire materials system using this flow law, compared the analytical /numerical results with experiments [e.g. Ref. 16, 18]. However, because of the complex nature of many of the systems studied *vis-à-vis* (1) the large spatial variation of interfacial shear stresses, and (2) the superposition of multiple deformation events, like creep of matrix and interface in a composite system, or film and interface in a film/substrate

system, the phenomenology of interfacial creep is difficult to accurately ascertain using the above methodologies.

C. PREVIOUS WORK

The difficulty and the discrepancies to isolate and accurately measure interfacial creep have been mentioned above. Recently, experiments to study the interfacial creep response in metallic composites in isolation from other concurrent effects were conducted in the Center for Materials Science and Engineering in NPS on model single fiber composites (SFC). Two different approaches were used, one using a fiber pushdown technique [Ref. 7, 8], and the other axial tensile loading on a specially designed SFC sample [Ref. 9].

Two different systems were used in the pushdown technique, one with limited mutual solubility (lead matrix / nickel fiber), a "diffuse" interface, and the other with no mutual solubility (lead matrix / quartz fiber) and therefore a sharp interface. The interface was uniformly loaded in shear during steady state sliding under constant pushdown loads. A direct measurement of the displacement of the fiber relative to the matrix revealed a threshold stress below which, interfacial sliding did not occur. The measured activation energy, on both systems, was somewhat less than that for grain boundary diffusion in the matrix. In addition, the stress exponent in the rate equation was equal to one. From those results it was concluded, that the interface slid by interface-diffusion-controlled diffusional creep. Further, scanning electron microscopy (SEM) of the interface Figure **5** revealed a periodic topography, consistent with the notion of local normal stress variation

along the interface due to a globally applied shear stress, as considered in the classical model for grain boundary sliding [Ref. 19].

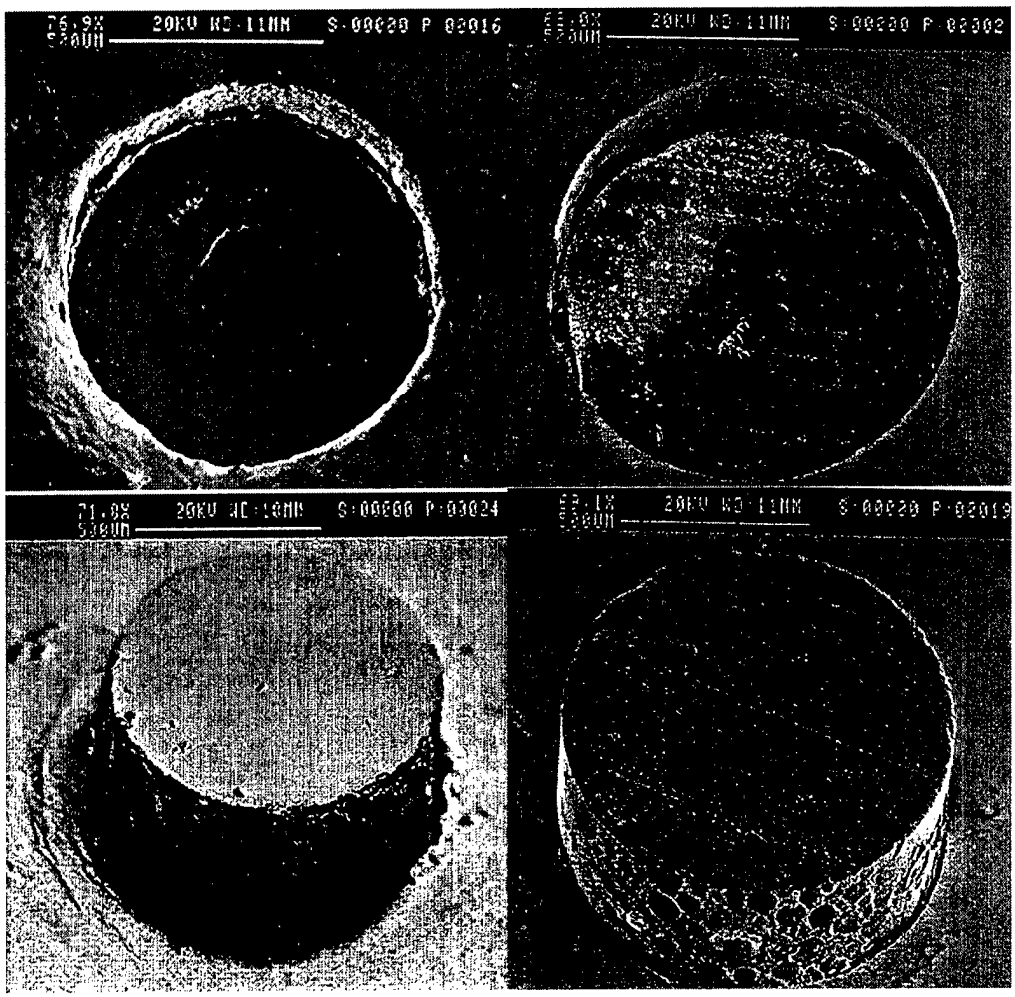

(a) (b)

Figure 5. Push-out tests of (a) Ni-fiber, (b) Quartz-fiber [Ref. 8]

The classical model for diffusional creep proposed by Raj and Ashby [Ref. 19], was modified to incorporate a global normal stress (in addition to the applied shear) in order to account for the effect of radial stresses which arise from CTE / Poisson's ratio

mismatch between the fiber and matrix. This continuum approach was able to account for a temperature-dependent threshold stress as a result of these thermal residual stresses [Ref. 7]. It was suggested that the interface for both model systems had adequate sources and sinks of vacancies. This inference was based on the observation that, the activation energy was found less than that of grain boundary diffusion and half the activation energy for lattice diffusion. The equation for the interfacial shear strain rate was represented as:

$$\dot{\gamma}_i = \frac{2D_m^{eff}\Omega\lambda}{kT\pi h^3}\left[\tau_i + \left(\frac{\pi h}{\lambda}\right)^3 \sigma_R\right] + \frac{4\delta_i D_i \Omega}{kTh^3}\left[\tau_i + 2\left(\frac{\pi h}{\lambda}\right)^3 \sigma_R\right] \qquad (1)$$

where τ_i is the shear stress acting on the interface, D_m^{eff} and D_i are the effective matrix and interface diffusivities, Ω is the atomic volume of the diffusive species (matrix), λ and h are the periodicity and width (i.e., twice the amplitude), respectively, of the interface, δ is the thickness of the interface, and σ_R is the normal (radial) stress acting on the interface. When $D_m^{eff} >> D_i$, the first item in equation 1 is negligible, and γ_i can be simplified as:

$$\dot{\gamma}_i = A_i(\tau_i + \tau_o) \qquad (2)$$

where τ_o, the contribution of the interfacial normal stress to sliding, is given by

$$\tau_o = 2\pi^3\left(\frac{h}{\lambda}\right)^3 \sigma_R \qquad (3)$$

and

$$A_i = \frac{4\delta_i D_{io}\Omega\lambda}{kTh^3}\exp\left[-\frac{Q_i}{RT}\right] \qquad (4)$$

where Q_i and D_{io} are the activation energy and frequency factor, respectively, for interfacial diffusion, k is the Boltzmann's constant, R is the gas constant, and T is the absolute temperature.

In equation 2, a compressive σ_R would result in a negative τ_o and hence result in a threshold behavior, whereas a tensile σ_R would increase the effective shear stress at the interface, and hence enhance the sliding rate. Equation 3 suggests that the temperature dependence of τ_o arises from the strong temperature dependence of the radial thermal residual stresses. From equation 4 is evident that diffusional creep would result in significant sliding rates only when h is small (i.e., when the interface is smooth). For composites containing fibers with rough surfaces (e.g., those produced via CVD), sliding by diffusional creep is probably inconsequential, unless Q_i is very low.

For the axial tensile creep tests, a specially designed lead matrix - nickel fiber single fiber composite (SFC) sample was used to investigate the effect of interfacial sliding. The sample design allowed (1) direct, separate measurement of the axial fiber and matrix strains, and (2) interfacial shear strains (and therefore interfacial sliding) to prevail within the gauge length [Ref 9]. The experimental results demonstrated a time dependent strain response of the matrix and fiber during constant force tensile creep testing. In Figure **6** is shown the differential strain between the matrix and the fiber. In all the samples, the matrix strain is observed to be larger than the fiber strain, indicating the occurrence of interfacial sliding. In the design of the test sample Figure 7, the openings in

the matrix were in such a position to provide 'free surfaces" and therefore artificial extremities, where interfacial shear stresses are expected to be large [Ref. 9]. This comes from the fact that typically sliding is confined to the ends of the tensile sample within the grip section, allowing the isostrain condition to be maintained over the tested gauge length. In this case, the composite creep rate decreases continuously and eventually vanishes as the applied load is progressively transferred from the matrix to the fibers. However, for large fiber diameters and short specimen lengths, sliding may occur within the gauge length, resulting in a violation of the isostrain condition.

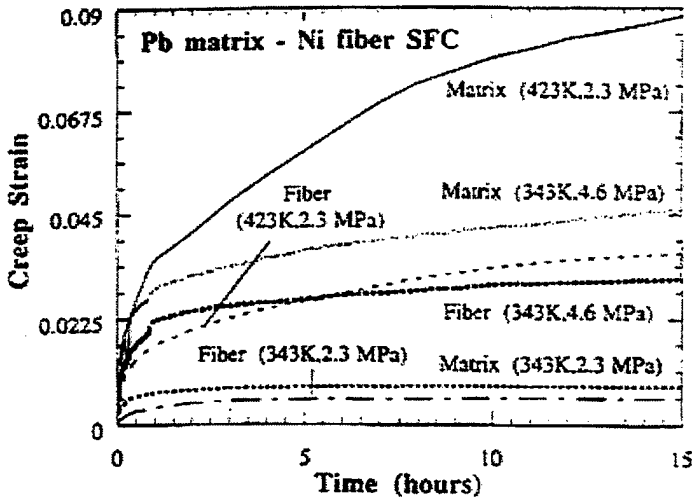

Figure 6. Differential matrix and fiber response during creep. [Ref. 9]

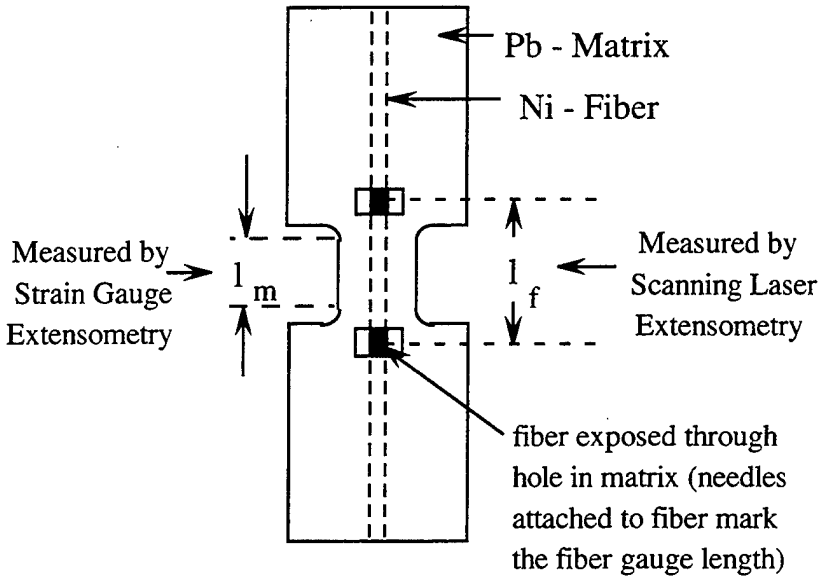

Figure 7. Schematic of the SFC sample used in constant load tensile creep experiments, [Ref. 9].

These results are significant, first, because they provide an alternate rationalization of threshold behavior during diffusional flow (besides interface-reaction-control [Ref. 13]), and may be useful in understanding creep in multi-phase systems with internal stresses. For instance, many dispersion strengthened systems where a threshold has been observed during diffusional creep have a large CTE mismatch between the matrix and the dispersion, thereby producing a strongly temperature-dependent radial compressive stress, which can result in a threshold behavior. Second, because isostrain violation and so differential strain rates between the matrix and the fiber are of particular importance during deformation in the absence of end-constraints, e.g. in axial creep of turbine blades, as well as during thermal cycling and flexural creep.

THIS PAGE INTENTIONALLY LEFT BLANK

III. OBJECTIVES

Several issues emerge from the preceding discussion. First, although interfacial sliding has generally observed in many systems and discussed in many studies, there is no general agreement on its mechanism. Second, there is confusion regarding the thermal residual stresses that result during fabrication, and as shown previously, may strongly affect the sliding kinetics via a threshold type effect. Third, because most mechanical tests utilized to date have not been expressly designed to study interfacial sliding, they result in complicated stress states at the interface, and therefore not well-suited for systematic studies of interfacial sliding. Finally, although interfacial sliding has often been invoked to rationalize the strain response of different materials, almost no systematic study of the impact of interfacial sliding on the overall deformation behavior of complete material systems has so far been conducted.

Therefore, the primarily objective of this study is to design an experimental approach that is capable of providing the necessary data regarding interfacial sliding at planar interfaces without being influenced by other mechanisms. The experimental setup is capable of testing specimens under shear and normal stresses independently and accurately control and measure the stress state at the interface.

The double-shear geometry of the sample was chosen to isolate (1) the effect of normal residual stresses by applying independently controlled normal loads at the interface and (2) to ensure loading of the interface by known uniform shear stresses.

In equations 3, 4 in the previous chapter we see that the width h and periodicity λ play an important role for the determination of the threshold stress and the interfacial

shear strain rate. In all the studies until now, values of both h and λ were assumed on observations after the fracture of the interface [Ref. 7, 8, 9, 17, 20]. With the present planar interface model the roughness of the bonded surfaces can be accurately controlled and test the validity of interfacial shear strain rate equation. Further, the ability to test simple model interfaces allows to systematically study the effect of interfacial "sharpness" by making samples under different processing conditions.

The study reported here are based on planar Al-Si interfaces, which have been diffusion-bonded under various conditions.

IV. EXPERIMENTAL PROCEDURE

A. SAMPLE PREPARATION

1. Double-Shear Geometry

In order to study the mechanical behavior of interfaces at high temperatures, shear stress experiments need to be conducted. Loading in pure shear is most of the times cumbersome. Experimental procedures involving torsion of thin-walled tubular specimens [Ref. 21] have been used but there were difficulties in determining the values of the true stress and true strain at any selected instant. To overcome these problems, the procedure of double-shear testing of bulk materials was introduced several years ago, as a method to obtain results with relatively simple equipment and quite fast [Ref 22].

Several experimental approaches simulating double-shear creep testing of bulk materials have been used throughout the years [Ref. 22, 23, 24] giving accurate results for measuring shear loading. Disadvantages that these techniques had, was the small specimen size, and the influence of bending stress arising from the double-shear loading. A better study for examining double shear specimens was produced by C. Mayr *et al* [Ref. 25] where they measured microscopic shear strains and were able to produce transmission electron microscopy (TEM) samples. The important advantages in using double-shear specimens were highlighted by I. Kazuhiko *et al* in their research [Ref. 26]. First, the fabrication is relatively easy that makes the procedure attractive for brittle materials such as silicon. Second, the experiments provide a direct measurement of true stress and true strain since there is no change in the cross-sectional area during testing.

Third, the tests maintain the conditions of true constant stress on the specimen without the requirement of incorporating a constant stress lever arm into the testing facility.

In the present study, for first time, double-shear geometry was utilized to test the strain response of planar interfaces. Figure **8** is showing how the combination of specimen and base geometry transfers the applied vertical load to pure shear stress along the interfaces.

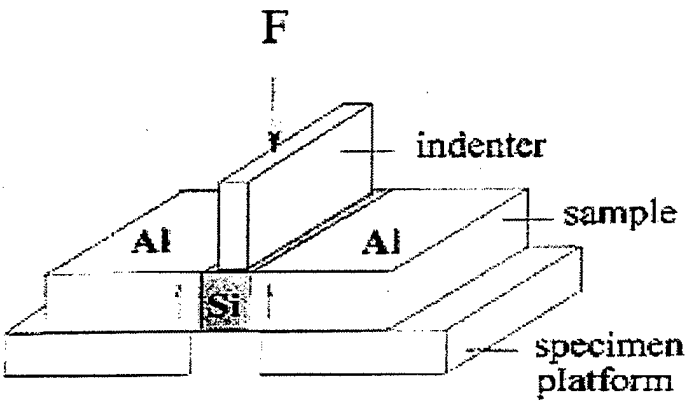

Figure 8. Representation of pure shear-loading specimen

The dimensions of the double-shear samples were carefully selected to minimize flexure of the specimen during testing. First, the ratio of the gap opening ($\mathbf{t_{gap}}$) to the width ($\mathbf{W_{Si}}$) of the Si, Figure **9**, was kept close to 1.1

$$\frac{t_{gap}}{w_{Si}} \approx 1.1. \qquad (1)$$

Secondly, the ratio of the thickness (**h**) of the sample to the gap opening was kept close to 0.8

$$\frac{h}{t_{gap}} \approx 0.8 \qquad (2)$$

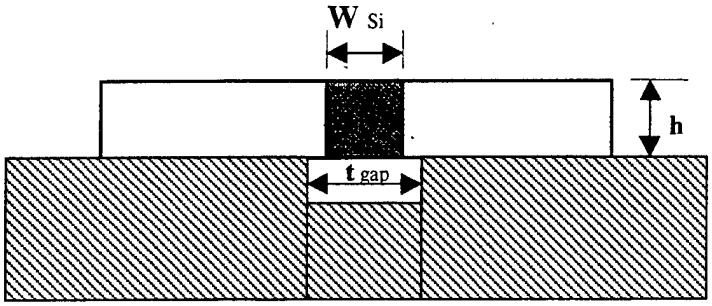

Figure 9. Schematic representation of the sample mounting

The numbers in equations 1, 2 were arrived from calculations based on the CTE mismatch by finite elements model (FEM) analysis reported in previous work [Ref. 8], where it was found that a $\frac{t_{gap}}{w_{Si}}$ ratio of at maximum 1.5 and a $\frac{h}{t_{gap}}$ ratio of at least 0.5 would result in minimal sample bending and in a uniform shear stress along the entire specimen thickness. In Figure 10**10**, a diffusion bonded Al-Si-Al specimen, ready for placing on the test base, is shown. Following sample fabrication, specimens were prepared, as described in section 3, to be appropriate for testing.

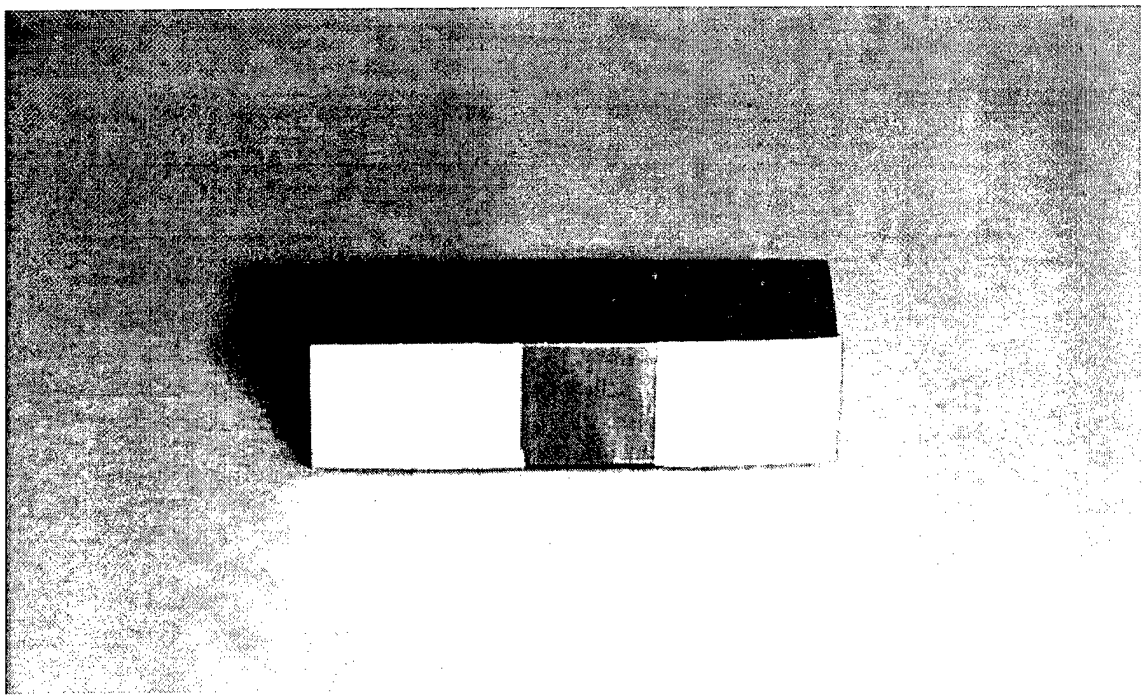

Figure 10. Diffusion Bonded Al-Si sample

2. System Selection

The double-shear geometry model described above, is fabricated by 99.99% pure Aluminum and undoped {100} Silicon. The choice of Al-Si system was introduced for four reasons: (1) Al and Si have limited mutual solid-solubility and hence allows production of interfaces with varying degrees of "sharpness", (2) the raw materials are readily available in both polycrystalline form and single crystals with different crystallographic orientations, (3) it is easy to fabricate diffusion bonding interfaces, (4) it is of practical importance in microelectronics. The phase diagram of Aluminum-Silicon system is shown in Figure **11**.

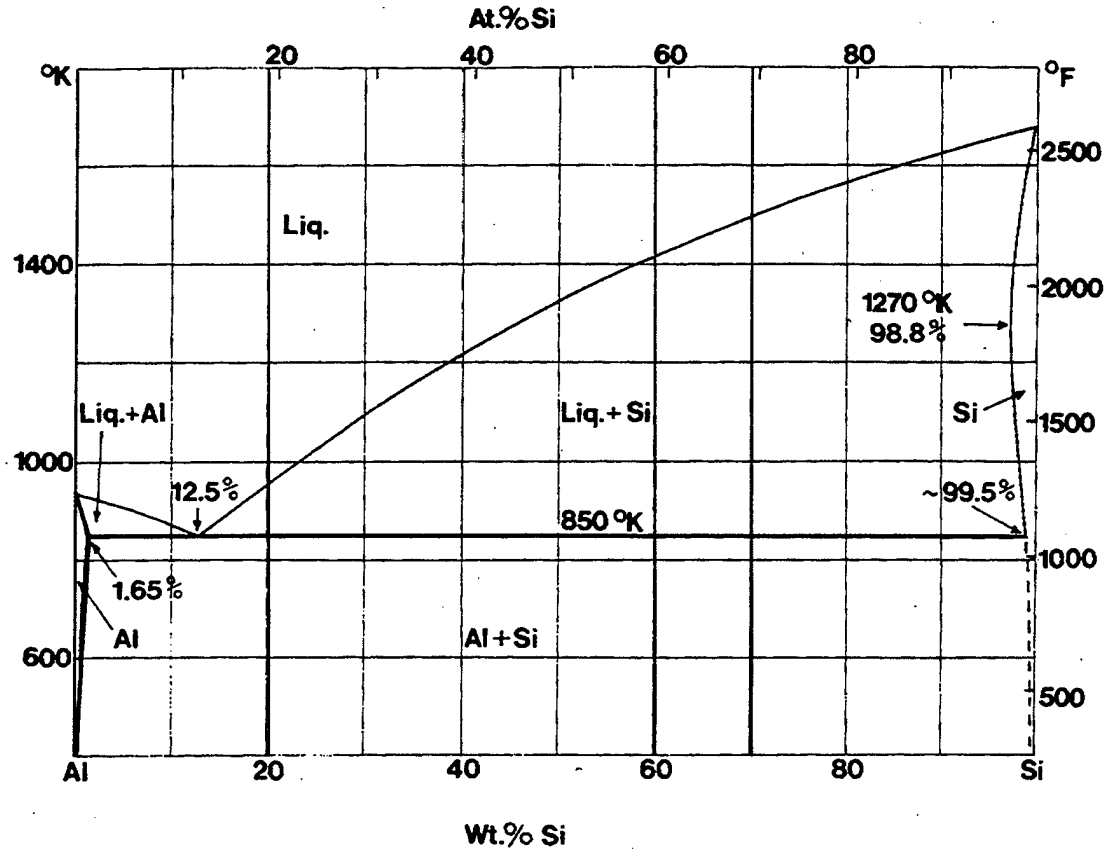

Figure 11. Al-Si Equilibrium-Phase Diagram [Ref. 27]

It is evident that there is limited solid-solubility of aluminum into silicon. On the other hand there is approximately 1.50wt% solid-solubility of silicon in aluminum at 565°C (silicon is the second most abundant impurity of aluminum) [Ref 27]. There is a eutectic composition at 577° C (850° K) with 12.5wt% silicon. From these information is clear that the Al-Si interface can be considered as "diffuse". Diffusion depth can be engineered to produce a sharp interface, by proper choice of temperature and time, as explained in section 3.b. The relevant thermal and mechanical properties of the constituent materials are delineated in table 1.

Property (at room temperature)	Aluminum	Silicon
σ_y (MPa) (Yield Strength)	18-24	128
ν (Poisson Ratio)	3	3
α (10^{-6}/K) (for 20-300°C) (Coefficient of Thermal Expansion)	25	2.33
T_m (K) (Melting Point)	933	2570

Table 1 Material Properties

3. Diffusion Bonding Procedure

The joining of metals to ceramics has been widely studied the last thirty years and extensive experiments have been contacted in order to explain the laws that describe those joining. The process of joining, in a simplified manner, is to bring the adherents (or the materials to be joined) into approximate geometry while in a transient high energy state and to allow the system to relax, or to dissipate this energy.

Diffusion bonding is a process in which two nominally flat surfaces are held together at an elevated temperature (usually above 0.6 of the absolute melting temperature of the least refractory of the two materials) for a period of time until a strong bond is formed. Diffusion bonding involves the interdiffusion of atoms across the interface of the adjacent materials [Ref. 28]. With diffusion bonding, joining is possible without the need of a foreign interlayer material acting as solder or brazing and therefore the introduction of at least two qualitatively different interfaces.

Diffusion bonding process is determined by three critical variables, (1) temperature, (2) pressure, and (3) time. As mentioned above temperature must be at least 60% of the most fusible material. The bonding pressure should ensure a tight contact

between the surfaces, and the holding time should be sufficient for an intimate contact to be formed and for diffusion processes to take place. When the two surfaces are brought into contact, they will first touch at their asperities. The pressure area will grow during the bonding process by mutual indentation of the asperities followed by the collapse of any interfacial voids at the interface as illustrated in Figure 12. After contact, local atomic rearrangement at the interface will transform it from two surfaces in contact into an interphase surface. The time required the two surfaces to come in contact, during diffusion bonding, is rate determining. In other words, the diffusion process of mass transport at the interface surfaces require more time than that responsible for transforming the now contacting surfaces into a grain boundary [Ref. 29].

In order to avoid the mentioned difficulties two different processes were used in the current study. First, a liquid phase process, incorporating a bottom purring technique,

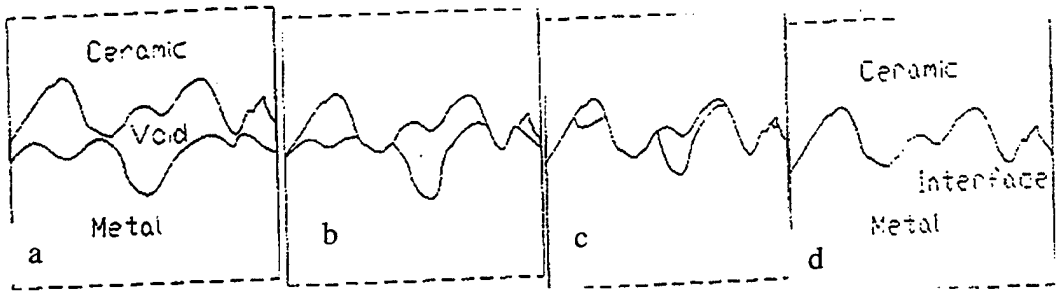

Figure 12. Schematic representation of diffusion bonded surfaces [Ref. 29]

was used to produce composite-like samples. Secondly, a traditional diffusion bonding technique in Argon atmosphere produced well-bonded samples, which was later used in the experimental procedure.

a. Liquid State Fabrication Procedure

In Figure **13**, drawings of the graphite molds used to melt Al are displayed. High purity (99,99%) aluminum in the form of small spheroids was melted using a cylindrical heating element from Watlow™ and a Variac transformer to control the temperature. Pure undoped silicon slices of 6mm thickness were made from a 4" diameter ingot with a 10" resin bonded diamond blade (from Buehler™). Pieces of 2.75"x1.25"x0.25" silicon were cut in a high-speed saw with high concentration diamond blades. These silicon pieces were mechanically polished up to 0.05μm.

Because of the high oxidation tendency of aluminum, stirring was necessary in order to achieve a nice liquid form and break all the oxide layers formed at the spheroids surfaces. In the bottom part of the mold, a silicon piece was placed inside the slot. Prior to pouring, slag (from the surface of the liquid) was removed in order to keep the solidified piece clean of impurities. By lifting the middle lever, pure aluminum liquid was poured, filling the space around the silicon. At the same time heating was turned off and the heater was removed to allow fast cooling of the graphite.

Two problems were identified with this method. First, due to the large CTE of aluminum, huge dimension changes produced extensive cracks on the silicon piece. Second, solubility of silicon in the liquid aluminum is high, therefore producing a large interphase layer of eutectic Al-Si alloy. The first problem was solved by modifying the dimensions of the silicon piece by isolating the liquid aluminum

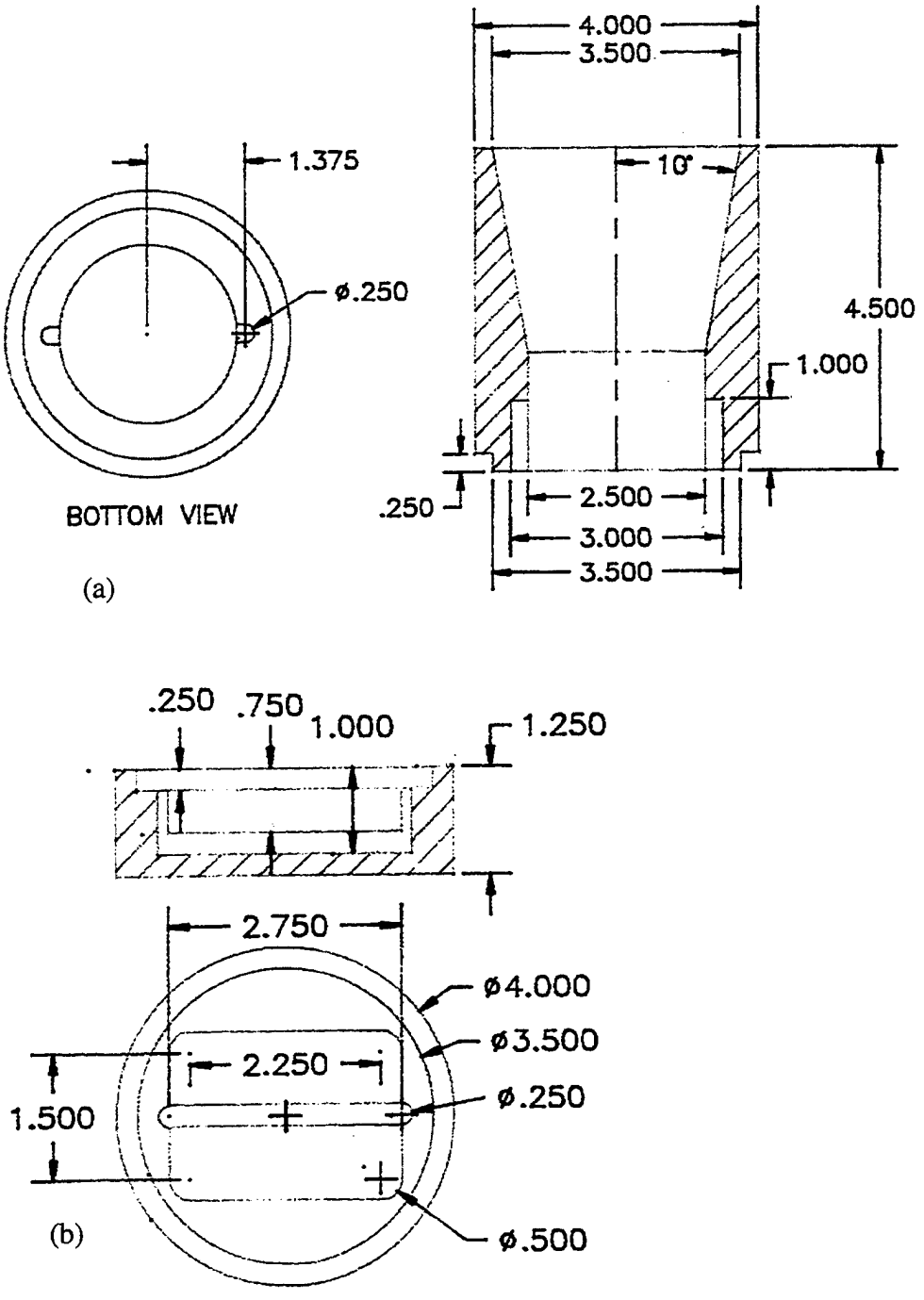

Figure 13. Graphite molds for the bottom purring technique (a) top part, (b) bottom part

during purring into two parts (contacting silicon only on the side surfaces). The second problem, however, was intractable in that even when the cooling rate was increased, there was still extensive diffusion of silicon into aluminum and the new interface was over a distance of 0.5 mm.

b. Solid State Fabrication Procedure

In order to achieve a sharp interface between the aluminum and silicon a diffusion bonding procedure at 565°C under Argon atmosphere was utilized. The temperature, which was slightly below the eutectic, was chosen to avoid a eutectic interlayer at the interface and assure good bonding. To achieve a sharp interface, diffusion time was kept to 1 $^1/_2$ hour and 2 hours. Samples were produced at both diffusion times. Figure **13** shows concentrations of aluminum and silicon across the interface of the 1.5-hour diffusion bonding time, based on energy dispersive X-ray spectroscopy (EDX) scan. As can be seen, diffusion depth was kept below 3μm, certifying the sharpness of the interface.

For the diffusion bonding samples, silicon pieces were cut in 15x20x5.5mm and aluminum in 18x24x10mm using the high-speed saw. Aluminum pieces were kept wider than silicon to avoid buckling and ensure uniform loading, and thus good contact over the entire interface. To avoid crack propagation on the silicon during pressing, silicon pieces edges were rounded and the surfaces were aligned to fit inside the aluminum.

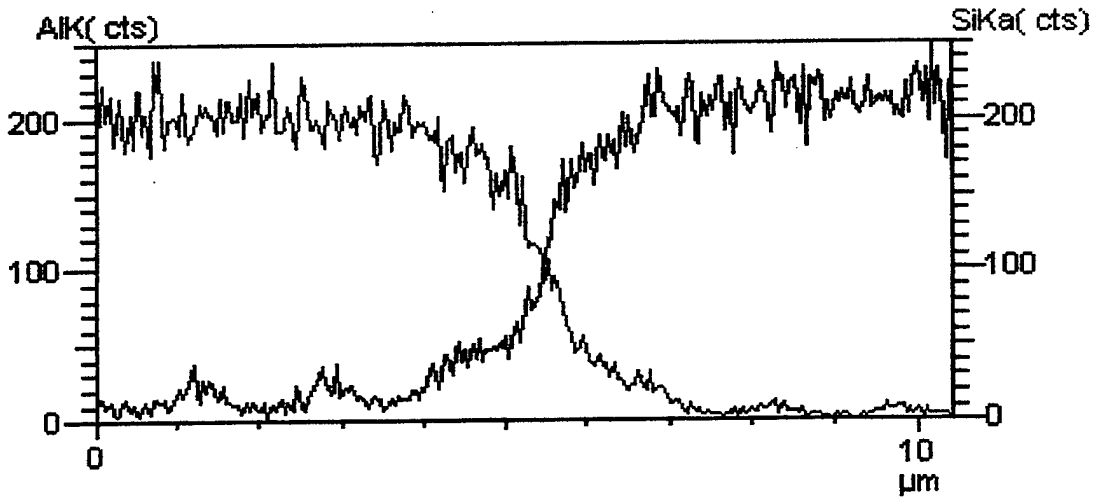

Figure 14. EDX of an interface after 1.5 hours diffusion bonding

Silicon was again mechanically polished, starting from a 1000 grit SiC paper, going up to 4000 grit, and then using water based diamond suspension of 6µm, 3µm, and 1µm on Microcloth™ and Texmet2000™ polishing cloths, all from Buehler Inc. Further polishing, up to 0.05µm was done with colloidal silica suspension. Aluminum pieces were also mechanically polished using SiC paper and diamond suspension up to 1µm, with the difference that no water was used as lubricant and ultra-sonic cleaning in a methanol bath was used between each step of polishing. Good sonic cleaning prior to start polishing with the diamond suspension was essential to prevent SiC abrasive particles from becoming embedded in the soft aluminum matrix, and to assure cleanliness of the polishing clothes. All the final polished surfaces (aluminum and silicon) were cleaned with methanol and dried with cold air.

A 2" c-clamp with high-carbon steel plates was used as a pressing device. Steel plates were covered with "Aerodag G" graphite spray, prior to contact with the

aluminum pieces, in order to avoid bonding between steel and aluminum. Proper alignment of the steel plates, aluminum and silicon pieces inside the c-clamp, was taken care in order to ensure even distribution of the load to the bonded surfaces.

A Lindberg™ furnace filled with ceramic bricks, to avoid large temperature fluctuations, was modified to accept the Argon piping for the artificial environment. Argon was supplied through two pressure regulators and dehumidifiers to ensure accuracy and cleanliness. Temperature monitoring was done with two extra thermocouples, one attached on the bonding specimen and the other on the bricks. After stabilization of the temperature at 565°C, the sample was inserted and the furnace was flushed with Argon for approximately two minutes.

The temperature of the sample was over 560°C in approximately ten minutes, and the flow of the Argon was decreased through a flow meter to 50-70 bubbles per minute. Kazakov [Ref. 28] in his recommendations for diffusion bonding of silicon and metals proposes that a heating rate of 50-60° C/minute and a cooling rate half that of heating, has been found to produce strong joints. In this study, cooling rates were between 30° C and 50° C/minute.

To avoid oxidization of the aluminum surface during the diffusion bonding process, after pressing the aluminum and silicon pieces together and prior to insert them into the furnace, the contacted surfaces were covered with an aluminum braze flux to reduce diffusion of oxygen atoms into the interface.

In Table 2 is a summary of the fabricated samples with the parameters and comments for the final product.

Sample #	Bonding Temperature (°C)	Bonding Time (min)	Comments
1, 3	570	30	Severe cracks on the Si with one surface not well bonded, cooling rate too high.
2	565	30	One surface not bonded.
4, 5	565	45	Severe cracks on the Si, high cooling rate.
6, 7, 8	565	60	Very weak diffusion bonded interface.
9,10,11,12	570	60	Weak diffusion bonded interface.
13,14, 15,16	565	90	Good diffusion bonded interface.
17,18	565	120	Good and strong diffusion bonded interface.

Table 2. Summary of diffusion bonded samples

4. Specimen Preparation

a. *Sectioning*

Following diffusion bonding, samples were grounded and polished to match the outside dimensions of aluminum and silicon. In this way, it was possible to mount the double shear sample into the holder to cut it into the dimensions mention in section 1. Sectioning a sample made of a very brittle and a very ductile material requires a low-speed saw, according to Ref 30. Using a low-concentration diamond blade, sectioning was possible at a speed between 2 and 3 RPM, without damaging the samples. In addition, to minimize stress variation along the sample, from the holder, thick aluminum foil was placed between the sample and the holder.

b. Mounting

In Figure 15 is shown the test base with the indenter over it. To mount the specimen so as to ensure enough clearance between the silicon and the edges of the gap/slot twisers had to be used. To hold it in place while heating and loading colloidal graphite and/or colloidal silver was placed at the ends of Al after placing it on the base. Also in the picture is shown the stepper-motor with the load cell used for applying the normal stresses at the interface as explained in section B.1.

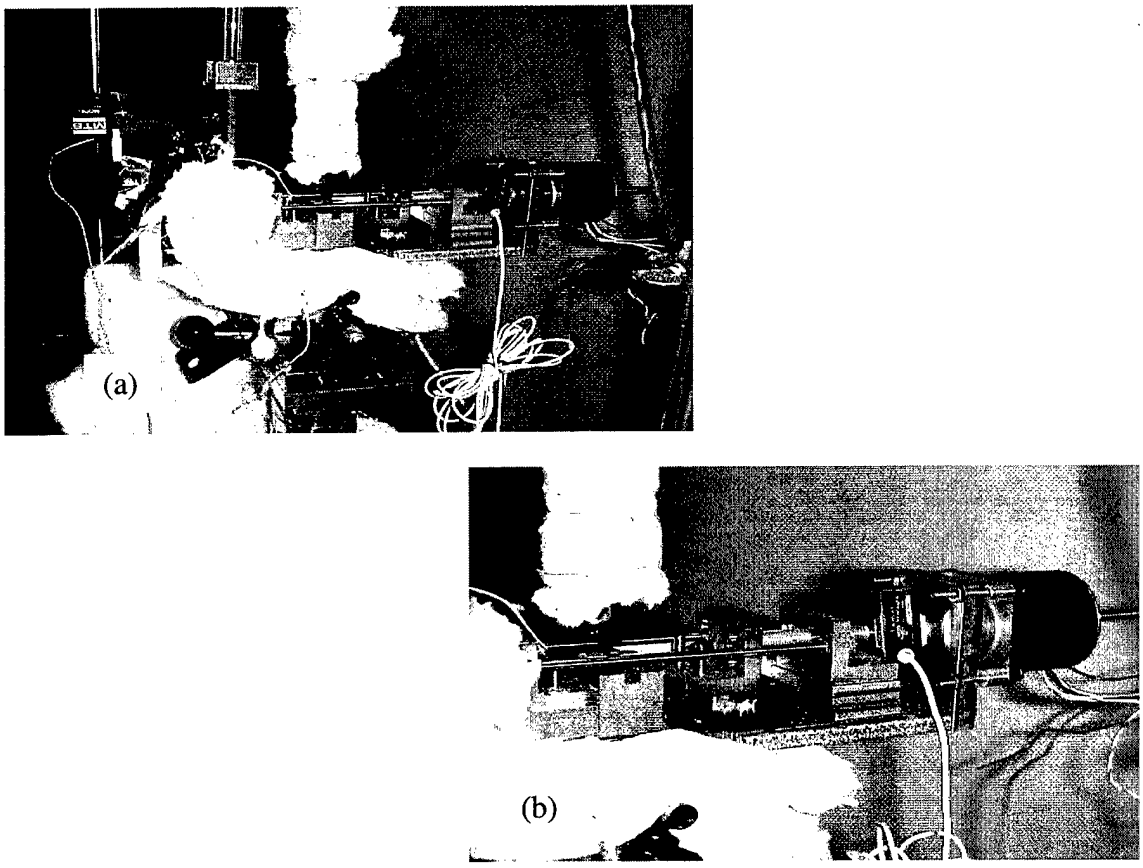

Figure 15. Views of testing device with specimen in place.

B. MECHANICAL TESTING

1. Apparatus

The experimental arrangement incorporates a plate-shaped tungsten (W) indenter mounted on a servo-hydraulic MTS frame equipped with the appropriate load cell and displacement gauges. The apparatus was used to apply a constant load to the top of the silicon, placing the two planar interfaces in pure shear, and monitor the silicon's top and bottom displacement, as a function of time. In addition to the shear stress, an extra load cell was located horizontally to apply a constant load normal to the interface.

In Figure **16** the MTS 810™ servo-hydraulic testing equipment is shown, along with all the peripherals used for the creep tests. On the left are the main supply, a digital display, the controller for the hydraulics, and the controller for the servo system. The outputs for RAM position (stroke), displacement (strain), and load are taken from the latter controller. The load cell (from MTS Systems Corp.) for the vertically applied load (Figure **16**) has four different ranges. The minimum range was used, giving a full scale of ± 224 Newton. Within this range, it was possible to measure the load with an error of less than ± 0.25N. The minimum range was also used for the extensometer (seen in Figure **15**a), also from MTS System Corp., where the resolution was $\pm 1\mu$m with a full scale of 0-0.5 millimeter. The second displacement sensor, placed under the Si, was a capacitance probe (from Capacitec™) with a resolution of 0.05μm and a full scale of 1.25 millimeters. Figure **17** shows a schematic representation of the testing setup with the position of the displacement and capacitance sensors.

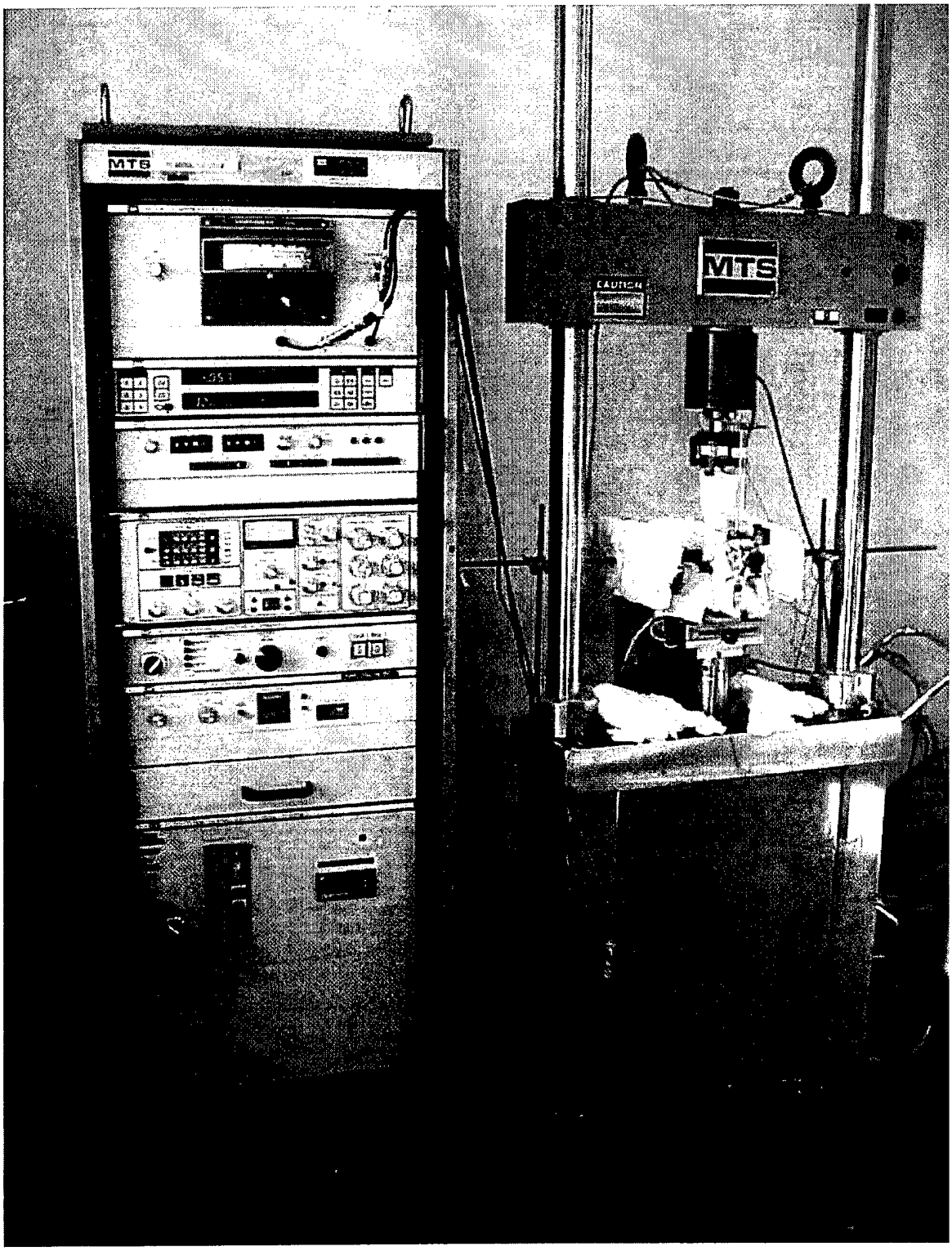

Figure 16. MTS frame with peripherals for creep testing

The displacement gauge was used to measure the top-face displacement of the silicon, while the capacitance gauge was used to measure the displacement of the silicon relative to the aluminum. The capacitance sensor was located inside the hot zone and it was able to withstand temperatures up to 700°C.

Figure **14** shows the stepper motor and the load cell for applying stresses normal to the interface. The stepper motor with its controller (from Anaheim Corp.) was able to perform very fine movement of the grip through a translation stage. The motor can withhold loads up to 800 Newton, while the load cell was able to measure tensile and compressive loads with an error less than ± 0.1N.

Experiments were conducted at two different temperatures. Heating of the specimen was possible through a pair of radiant strip heaters (shown in Figure **16**) able to achieve temperatures up to 400°C, and controlled from a programmable proportional controller with a control band $\pm 1^{o}$C, all from Watlow Inc. To achieve temperatures over 100°C and to maintain that temperature constant, thermal insulation, covering the whole testing device was necessary.

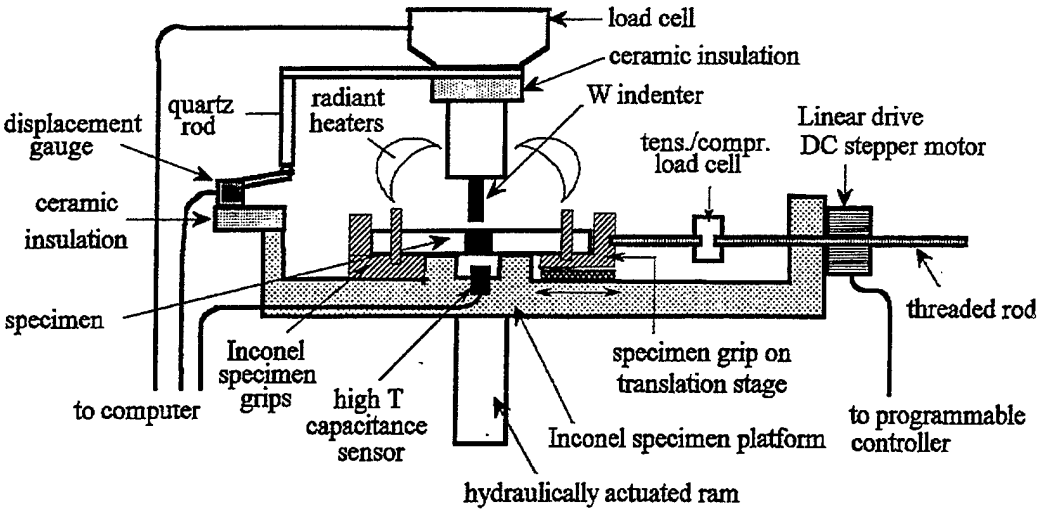

Figure 17. Schematic representation of the testing equipment

In order to maintain both load cells outside the hot zone, ceramic insulation (alumina/mullite) was placed between the tungsten indenter and the vertical load cell while the horizontal (tension/compression) cell was left outside the covered area.

To ensure uniform distribution of the load on the silicon a small, 4mm-wide, tungsten plate was placed over it. This was the loaded area of the W-indenter. The specimen platform was on a micrometer controlled X-Y translation stage to ensure alignment of the silicon directly under the indenter.

The experimental setup allows flexibility in the tests that can be performed. In addition to the push-out and creep tests, stress relaxation tests may be performed using the apparatus. Further, the ability to independently load the interface in shear, as well as normally, offers two capabilities. First, it allows to study the role of interfacial normal stress in diffusional creep, e.g., threshold behavior in compression and acceleration in

tension, as indicated in the work of Ref. 8. Second, it gives the ability to study the dependence of the operative sliding mechanism on the ratio of shear to normal stresses (for instance, when the interface is loaded in shear only, the mechanism may be either diffusional creep [Ref. 7, 8, 10, 17], or dislocation creep due to movement of interface dislocations [Ref. 14, 15, 31], whereas when the interfacial stress has a large normal component, sliding may be controlled by glide of lattice dislocations in a narrow shear band near the interface [Ref. 36]).

2. Data Acquisition

The data collected during these experiments were acquired using an Apple Macintosh™ computer containing a Strawberry Tree™ data acquisition card. The Strawberry Tree Workbench™ software was utilized to control the data recording and to provide a real time display of the data as it was collected. The raw data was analyzed using the graphic software, Kaliedagraph™.

3. Pushout Testing

Push-out tests in composites, are constant displacement rate tests during which the reinforcement (usually fiber) is pushed out of the matrix and the load required to effect the displacement is continuously monitored [Ref. 37, 38]. They can involve simultaneous application of axial in-plane tension [Ref. 39, 40], or not. All these studies have shown that push-out tests can be successfully utilized to determine the shear strength characteristics of the interface.

The push-out test was conducted with the servo-hydraulic system, in strain control mode, using the same setup as in the creep tests (Figure **17**). Figure **18** shows the load versus time during a push-out test, up to fracture point. The test was conducted at 150°C and the fracture point was designated as P_f. The fracture load was normalized to an average fracture interfacial shear stress τ_f, which is determined as:

$$\tau_f = \frac{P_f}{A}$$

where A is the total surface area of the interface (including both sides of silicon). The maximum load recorded during the test prior to fracture (P_f) is indicative of the strength of the interface, which was determined to be ~2.8Mpa.

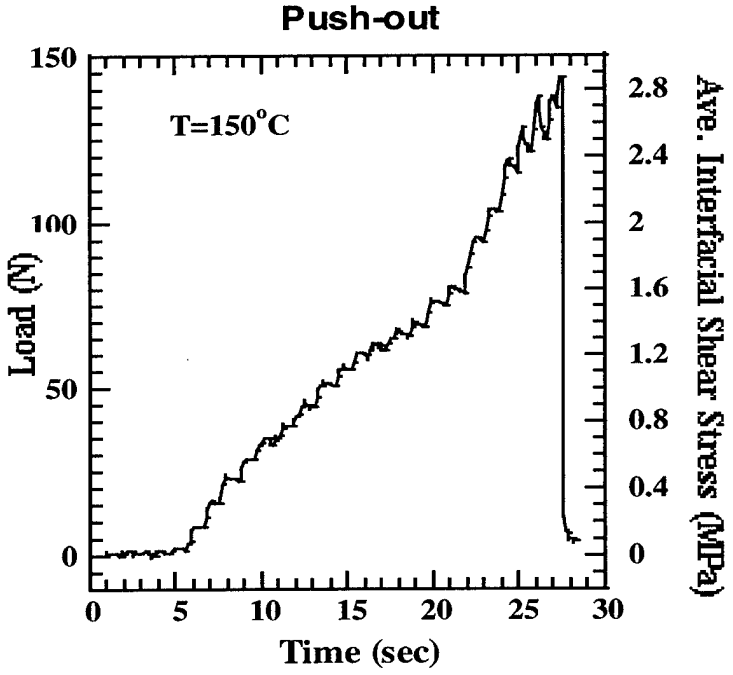

Figure 18. Load versus time during the push-out test

The objective of the push-out test was to determine the maximum stress that can be applied without causing fracture along the interface. This information was necessary to determine the proper loads that should be applied during the creep tests in order to measure the creep response of the interface without causing fracture.

4. Creep Testing

A few preliminary creep curves were generated to demonstrate the operation of the equipment. Tests were conducted at various stress levels, below the maximum stress τ_f, and at various temperatures. During these tests, the MTS system was in load control mode, and a constant load was maintained with accuracy ± 0.01 MPa.

Figure **19** shows an example of the creep response of the diffusion bonded Si-Al interface at 150°C at three different stresses versus time. Clearly, the differences in the creep rates are apparent, despite the scatter of the data due to the signal-to-noise ratio limitations. These data represent the top-face displacement only, and may include any creep displacement of the Al-matrix in addition to creep of the interface. Figure 20 shows both top-face and bottom-face displacement. Both displacements show identical trends, indicating that the contribution of the matrix creep to the measured displacement is minimal. Most of the measured displacement arises due to interfacial creep. Further work is necessary to determine whether the sliding occurs entirely at the interface, or whether in a narrow band of the matrix next to the interface.

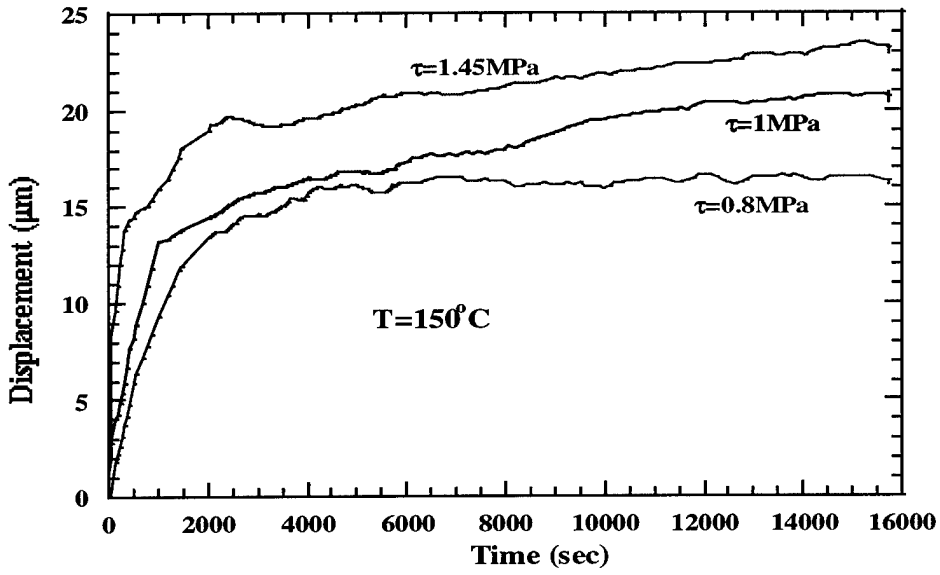

Figure 19. Creep response at three different stress levels.

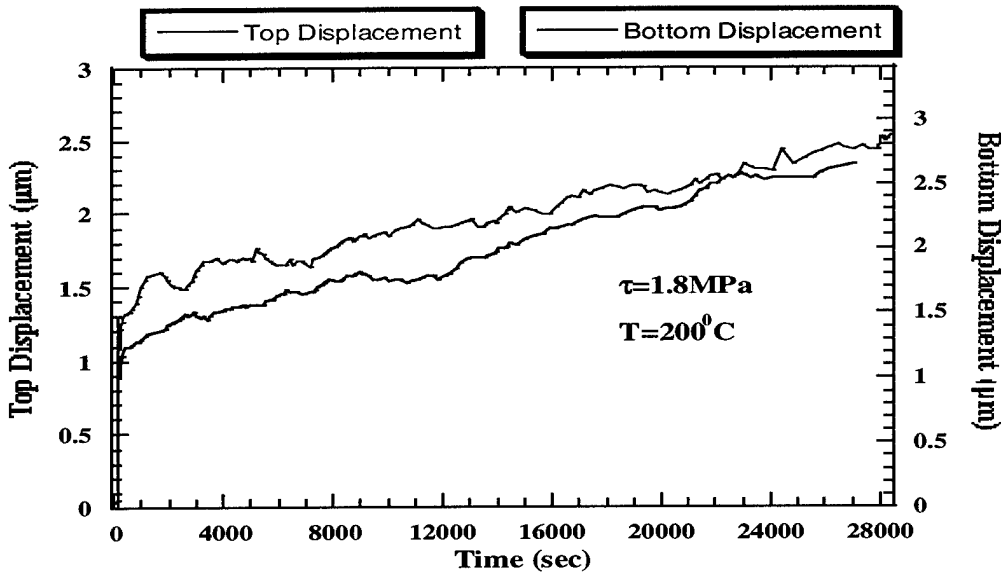

Figure 20. Top and bottom displacement versus time. Note the creep rate is almost identical meaning that there is no creep of the Al-matrix involved in this example.

C. CHARACTERIZATION OF THE INTERFACE

1. Scanning Electron Microscopy (SEM)

To determine the creep response of the interface is necessary to study the nature of the interface prior and after deformation. A preliminary work was done by examining most of the specimens in a Scanning Electron Microscope (SEM) prior to deformation, to determine whether the model used by Raj and Ashby [Ref. 19] was valid, and to examine the nature of the diffusion bonded interface. Figure **21** shows two SEM micrographs in different magnifications, (a) at 83.5 times, and (b) at 3050 times (aluminum is the part with the rough-look). From Figure 21(a) we see the sharpness of the interface and from Figure 21(b) the width h and periodicity λ can easily be calculated to match the wave-like model proposed in Ref. 19. In Figure 21(b) can be also seen a microvoid with less than 1μm diameter. In total, those microvoids was found to be less than 1% of the total interface.

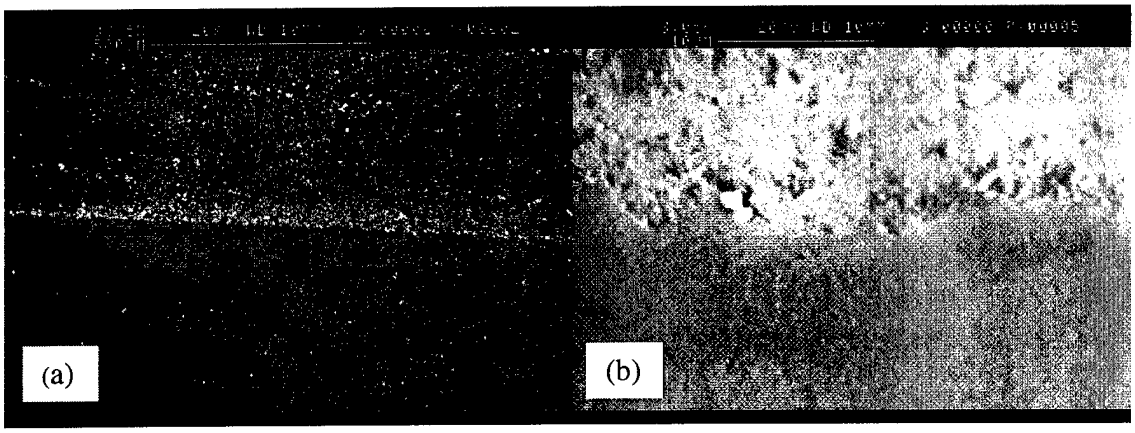

Figure 21. SEM micrographs showing the Al-Si interface before creep. In (b) a microvoid can be seen that is less than 1μm diameter.

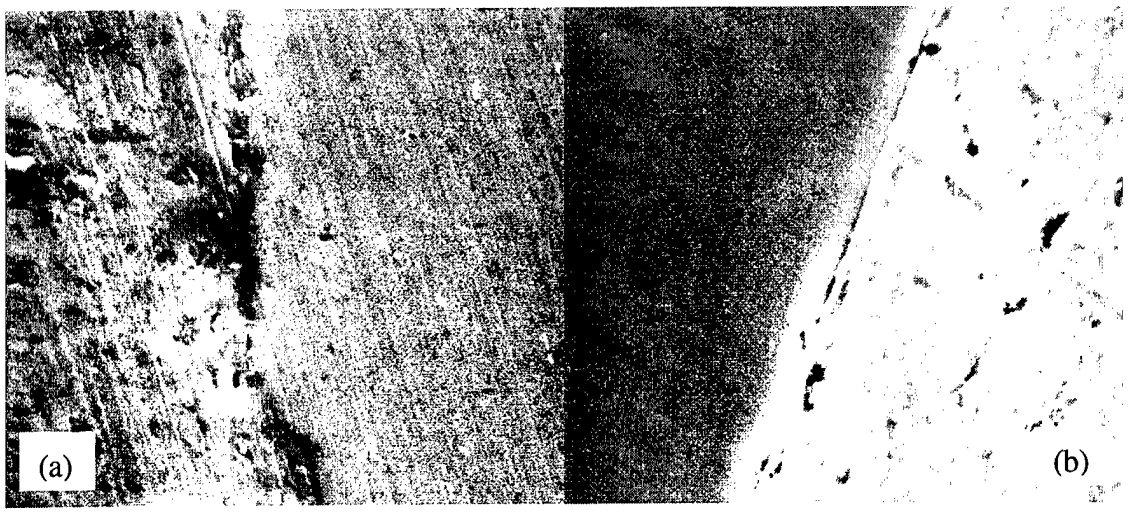

Figure 22. SEM migrograph of the Al-Si interface at two different magnifications, (a) 2000x, (b) 1500x.

Figure **22** shows the interface of a different specimen. The sharpness of the interface is obvious and the good bonding is assured at the 2000 times magnification. Producing different surface 'roughness' (by various polishing depths) will give different values for h, λ and will further proof the theory of diffusion controlled interfacial sliding proposed by Funn *et al.*

V. CONCLUSIONS

An experimental technique to study the characteristics of planar interfacial creep has been developed along with diffusion bonded samples of aluminum and silicon. The diffusion bonding technique produced a sharp interface, as can be seen from the SEM micrographs.

In order to study the creep response of the planar interface under pure shear and controlled normal stresses, a double shear specimen geometry was utilized. The diffusion bonding technique used here can provide us with the critical information of the width h and periodicity λ for the determination of the threshold stress and the interfacial shear strain rate. The surface 'roughness' of silicon was found to remain the same after the diffusion bonding process, so that the values of h and λ for the bonded interface can be determined from the surface profile of silicon prior to bonding. The specimen dimensions were carefully selected to minimize flexure and assure uniform shear stress along the interface during push-down creep testing.

The experimental set-up is suitable for both constant displacement-rate and constant load creep tests, and can measure both top-face and bottom-face displacement of the phase during push-down testing. From this, it is capable of measuring the interfacial displacement (both instantaneous and time-dependent) with high precision, and thus allows the study of interfacial sliding in isolation from concurrently operative superimposed deformation mechanisms. In the current tests, the interface was sliding under pure shear without any evidence of fracture or debonding. Clearly, the results show interfacial sliding via time-depended relaxation mechanisms. Further tests will need to

collect a larger data set in order to allow the determination of the exact type of creep operative in various stress-temperature regimes.

LIST OF REFERENCES

1. Chawla, K. K., *Composite Materials*, Springer-Verlag, New York, 1998.

2. Ashby, M. F., *A First Report on Deformation-Mechanism Maps*, Acta Metallurgica, (1972), **20**, pp.887-897.

3. Ashby, M. F., and H. J. Frost, *Deformation Mechanisms Maps*, Pergamon Press, Oxford, UK, 1982.

4. Dutta, I. S. Mitra, and A. D. Wiest, *Residual Stresses in Composites-Measurements, Modelling and Effects on Thermo-Mechanical Behavior*, E.V. Barrera and I. Dutta, TMS-AIME, (1993), pp.273.

5. Yoda, S., N. Kurihara, K. Wakashima, and S. Umekawa, *Thermal Cycling Induced Deformation of Fibrous Composites with Particular Reference to the Tungsten-Copper System*, Metallurgical Transactions, (1978), **9A**, pp.1229-1236.

6. Mitra S., I. Dutta, and R. C. Hansen, Journal of Material Science, (1991), **26**, pp.6223.

7. Funn, J., V., and I. Dutta, *Creep Behavior of Interfaces in Fiber Reinforced Metal-Matrix Composites*, Acta Metallurgica et Materialia, (1999), **47**, pp.149-164.

8. Funn, J., *Creep Behavior of the Interface Region in Continuous Fiber Reinforced Metal-Matrix Composites,* Master's Thesis, Naval Postgraduate School, Monterey, CA, September 1997.

9. Nagarajan, R., I. Dutta, J. V. Funn, and M. Esmele, *Role of interfacial sliding on the longitudinal creep response of continuous fiber reinforced metal-matrix composites,* Materials Science and Engineering, (1999), **A259**, pp. 237-252.

10. Zhmurkin, D. V., T. S. Gross, and L. P. Buchwalter, *Interfacial Sliding in Cu/Ta/Polyimide High Density Interconnects as a Result of Thermal Cycling*, Journal of Electronics Materials, (1997), **26**, pp.791-797.

11. Shen, Y. L. and S. Suresh, *Steady-State Creep of Metal-Ceramic Multilayered Materials*, Acta Metallurgica et Materialia, (1996), **44**, pp. 1337-1348.

12. Mishra, R. S., T. R. Bieler, and Mukherjee, *Mechanism of High Strain rate Superplasticity in Aluminum Alloy Composites*, Acta Metallurgica et Materialia, (1997), **45**, pp.561-568.

13. Arzt, E., M. F. Ashby, and R. A. Verall, *Interface Controlled Diffusional Creep*, Acta Metallurgica et Materialia, (1983), **31**, pp. 1977-1989.

14. Dlouhy, A., N. Merk, and G. Eggeler, *A Microstructural Study of Creep in Short Fiber Reinforced Aluminum Alloys,* Acta Metallurgica et Materialia, (1993), **41**, pp. 3245-3256.

15. Dlouhy, A., N. Merk, and G. Eggeler, *A Micromechanical Model of Creep in Short Fiber Reinforced Aluminum Alloys*, Acta Metallurgica et Materialia, (1995), **43**, pp. 535-550.

16. Kim, K. T., and R. M. McMeeking, *Power Low Creep with Interface Slip and diffusion in a Composite Material*, Mechanics of Materials, (1995), **20**, pp. 153-164.

17. Jobin, V. C., R. Raj, and S. I. Phoenix, *Rate Effects in Metal-Ceramic Interface Sliding from the Periodic Film Cracking Technique*, Acta Metallurgica et Materialia, (1992), **40**, pp. 2269-2280.

18. Nimmagada, P. B. R., and P. Sofronis, *Creep strength of Fiber and Particulate Composite materials: The effect of Interface Slip and Diffusion*, Mechanics of Materials, (1996), **23**, pp. 1-19.

19. Raj, R. and M. F. Ashby, *On Grain Boundary sliding and Diffusional Creep*, Metallurgical Transactions, (1971), **2**, pp.1113-1127.

20. Dutta, I., *Role of Interfacial and Matrix Creep During Thermal Cycling of Continuous Fiber Reinforced Metal-Matrix Composites*, Acta Materialia, in press, (accepted October 1999).

21. Browne, R. J. D. Lonsdale, and P. E. J. Flewitt, *Multiaxial Stress Rupture Testing and Compendium of Data for Creep Resisting Steels*, Journal of Engineering Materials Technology, ASME Transactions, (1982), **104**, pp. 291-296.

22. Schwartz D. M., J. B. Mitchell, and J. E. Dorn, *The Mechanism of Prismatic Creep in Mg-12at% Li*, Acta Metallurgica et Materialia, (1967), **15**, pp.485-490.

23. Matsuda, A., *The Plastic Deformation of Iron Single Crystals with Shear Tests in {110<111> and {112<111> Slip Systems*, Transactions of Japan Institute of Metallurgy, (1977), **18**, pp.214-220.

24. Funk, W., and E. Blank, *Shear Testing of Monocrystalline Alloys Incorporating the Measurement of Local and Integral Strains,* Material Science and Engineering, (1984), **67**, pp. 1-11.

25. Mayr, C., G. Eggeler, G. A. Webster, and G. Peter, *Double Shear Creep testing of Superalloy Crystals at Temperatures Above 1000 °C,* Material Science and Engineering A, (1995), **199**, pp.121-130.

26. Kazuhiko, I., H. Zenji, F. Takayoshi, S. Takeshi, N. Minoru, M. Yan, and L. G. Terence, *A New Miniature Mechanical Testing Procedure: Applications to Intermetallics*, Metallurgical and Materials Transactions A, (1997), **28A**, pp.2577-2582.

27. Mondolfo, L. F., *Aluminum Alloys*, Butterworths, London, 1976.

28. Kazakov, N. F., *Diffusion Bonding of Materials*, Mir Publishers, Moscow,1985.

29. Derby, B., *The Formation of Metal-Ceramic Interfaces by Diffusion Bonding*, Proceedings of an International Workshop, Pergamon Press, (1989), pp. 161-167.

30. Buehler, *Technical Manual*, 1992

31. Hsiung, L. M., and T. G. Nieh, *Creep Deformation of Lamellar TiAl Alloys Controlled by Viscous Glide of Interfacial Dislocations*, Interstitial and Substitutional Solute Effects in Intermetallics, I. Baker, R. D. Noebe and E. P. George (editors), TMS, (1998), pp. 201-210.

32. Ignat, M. and R. Bonnet, *Role of the Phase Boundaries in the Hot Deformation in Tension of Al-$CuAl_2$ Single Eutectic Grains- A Deformation Model*, Acta Metallurgica et Materialia, (1983), **31**, pp.1991-2001.

33. Mori, T. K. Tanaka, Y. Nakasone, J. Huang, and M. Taya, *Creep of a Metal-Matrix Composite with or without Diffusion and Sliding on Matrix/Reinforcement Interfaces*, Key Engineering Materials, (1997), **127-131**, pp.1145-1152.

34. Meyer, D. W., R. F. Cooper, and M. E. Plesha, *High Temperature Creep and the Interfacial Mechanical Response of a Ceramic Matrix Composite*, Acta Metallurgica et Materialia, (1993), **41**, pp.3157-3170.

35. Ashby, M. F., *On Interface-Reaction Control of Nabarro-Herring Creep and Sintering*, Scripta Metallurgica, (1969), **3,** pp. 837-842.

36. Soyez, G., G. Elssner, M. Ruhle, and R. Raj, *Constrained Yielding in Niobium Single Crystals Bonded to Sapphire*, Acta Metallurgica et Materialia, (1998), **46**, pp.3571-3581.

37. Welhs, T. P., and W. D. Nix, *Experimental examination of the Push-Down Technique for Measuring the Sliding Resistance of Silicon Carbide Fibers in a Ceramic Matrix*, Journal of the American ceramic Society, (1991), **74-3**, pp. 524-534.

38. Kalton, A. F., C. M. Ward-Close, and T. W. Clyne, *Development of Tensioned Push-out Test for study of Fiber/Matrix Interfaces*, Composites, (1994), **25-7**, pp.637-644.

39. Watson, M. C., and T. W. Clyne, *The Tensioned Push-out Test for Fiber-Matrix Interface Characterization Under Mixed Mode Loading*, Materials Science and Engineering, (1993), **A160**, pp. 1-5.

40. Kalton, A. F., D. B. Miracle and T. W. Clyne, *The Effect of Interfacial Strength on the response of Ti MMCs to Single Fiber Push-out and Trensverse Tensile Testing*, Key Engineering Materials, (1997), **127-131**, pp.659-670.

THIS PAGE INTENTIONALLY LEFT BLANK

INITIAL DISTRIBUTION LIST

1. Defense Technical Information Center 2
   8725 John J. Kingman Rd., STE 0944
   Ft. Belvoir, Virginia 22060-6218

2. Dudley Knox Library 2
   Naval Postgraduate School
   411 Dyer Rd.
   Monterey, California 93943-5100

3. Department Chairman, Code ME/Mc 1
   Department of Mechanical Engineering
   Naval Postgraduate School
   700 Dyer Rd., Bldg. 245
   Monterey, California 93943-5100

4. Professor Indranath Dutta, Code ME/Du 2
   Department of Mechanical Engineering
   Naval Postgraduate School
   700 Dyer Rd., Bldg. 245
   Monterey, California 93943-5100

5. Ioannis Farsaris, ... 3
   4 Prince George St.,
   Agios Nikolaos,
   Crete, 72100,
   Greece

6. Embassy of Greece 1
   Naval Attaché
   2228 Massachusetts Avenue, NW
   Washington, D.C. 20008

7. Naval/Mechanical Engineering, Code 34 1
   Naval Postgraduate School
   700 Dyer Rd., Bldg. 245
   Monterey, California 93943-5100